

1 **Quantifying the environmental controls on erosion of a hard rock cliff**

2

3 **Authors:**

4 Vann Jones (née Norman) E.C.*, N.J. Rosser, M.J. Brain, and D.N. Petley

5 *Corresponding author: e.c.vann-jones@dur.ac.uk Tel: +44 191 334 1843

6

7 **Affiliation:**

8 Institute of Hazard, Risk and Resilience, Department of Geography, Durham University, Lower
9 Mountjoy, South Road, Durham, DH1 3LE, UK.

10

11 **Abstract:**

12 Linking hard rock coastal cliff erosion to environmental drivers is challenging, with weak
13 relationships commonly observed in comparisons of marine and subaerial conditions to the
14 timing and character of erosion. The aim of this paper is to bring together datasets to explore how
15 best to represent conditions at the coast and to test relationships with erosion, which on this coast
16 is primarily achieved via rockfalls. On the N. Yorkshire coast in the UK we compare a continuously
17 monitored microseismic dataset, regionally monitored coastal environmental conditions,
18 modelled at-cliff conditions and periodic high-resolution 3D monitoring of changes to the cliff face
19 over a 2-year period.

20 Cliff-top microseismic ground motions are generated by a range of offshore, nearshore and
21 at-cliff sources. We consider such ground motions as proxies for those conditions that promote
22 the occurrence of rockfalls and erosion. Both these data and modelled at-cliff water levels provide
23 improved insight into conditions at, and wave energy transfer to, the cliff. The variability in
24 microseismic, modelled and regionally-monitored environmental data derives statistically

25 significant relationships with increases in the occurrence of rockfalls. The results demonstrate a
26 marine control on the total volume and size characteristics of rockfalls. The strongest
27 relationships found are with rockfalls sourced from across the entire cliff, rather than just at the
28 toe, indicating that the marine influence, albeit indirectly, extends above and beyond the area
29 inundated. These results identify failure mechanisms driving erosion, where a range of processes
30 unique to the coast trigger failure, but in a manner beyond purely wave action at the cliff toe.

31 Greater erosion occurs at the cliff toe. However, comparing water level inundation
32 frequency, microseismic energy transfer and erosion, we observe that heights up the cliff that
33 correspond with water levels associated with low frequency, high energy storms, or more
34 frequent inundation, do not experience increased erosion. Our results describe the relationship
35 between inundation duration, energy transfer and erosion of hard rock cliffs, and illustrate the
36 relative intensity of erosion response to variations in these conditions. Implicitly our data
37 suggests that in future, cliffed rocky coasts may be relatively quick to respond to changes in
38 environmental forcing.

39

40 **Key words:** Rocky coast, Coastal erosion, Coastal cliff, Cliff ground motion, Rockfall, Wave energy.

41

42 **1 Introduction**

43 Few studies have attempted to quantify the controls on hard rock cliff erosion compared to
44 cliffs of softer materials, likely due to comparatively slow response to environmental forcing and
45 the difficulties of monitoring steep, hard rock cliffs. The development of high-resolution
46 monitoring techniques, such as terrestrial and airborne laser scanning, has begun to address this
47 (e.g. Sallenger et al., 2002; Lim et al., 2005; Rosser et al., 2005; Collins and Sitar, 2008; Young et al.,
48 2011a), though establishing links between observed erosion and concurrent environmental
49 conditions remains problematic.

50 Monitoring demonstrates that coastal rock cliff erosion is in part a function of mass
51 wasting via spalling, rockfalls (e.g. Lim et al., 2010), block falls and topples (e.g. Young et al.,
52 2011a). Failures from rock cliffs have been observed to be sourced from locations across the
53 whole cliff face, and many actively eroding non-carbonate coastlines often lack a concave toe
54 notch considered indicative of marine erosion (Pierre and Lahousse, 2006; Rosser et al., 2007;
55 Young et al., 2009a). The propagation of rockfalls has been observed to facilitate the transmission
56 of marine erosion up the cliff face over time (Rosser et al., 2013). Combined, these observations
57 suggest a complex and variable interplay of geological and environmental controls on erosion. For
58 example, whilst previous work has shown a close link between rockfall geometry and geology
59 (Duperret et al., 2002; Kogure and Matsukura, 2010), analysis of the timing of rockfalls with
60 energetic environmental conditions yields only poor correlations (Rosser et al., 2007; Lim et al.,
61 2010). Encouragingly, high-resolution studies of soft rock cliffs have had more success in linking
62 the occurrence of failure to specific drivers, such as extreme wave runup (Sallenger et al., 2002;
63 Collins and Sitar, 2008) and rainfall (Collins and Sitar, 2008; Young et al., 2009b; Brooks et al.,
64 2012). By implication either harder rock coasts do not respond rapidly to forcing, their response
65 is lagged, or current monitoring data is incapable of capturing these relationships.

66 In the absence of data on conditions proximal to the coast, it has been common practise to
67 approximate often far-field observations of marine and weather conditions, using numerical
68 transformations or interpolations, as the basis for comparisons between erosion and its drivers
69 (Ruggiero et al., 2001; Collins and Sitar, 2008; Young et al., 2009b). Transformations to estimate
70 wave power propagation and dissipation have been used to estimate marine erosive capability
71 (Stephenson and Kirk, 2000; Trenhaile and Kanyaya, 2007), and drive models of long-term
72 (millennial-) coastal evolution (e.g. Trenhaile, 2000; 2011). The transformation or indeed the
73 direct measurement of wave characteristics to explain short-term (< monthly) rock cliff erosion
74 remains more problematic (Lim et al., 2010).

75 There has been a significant amount of numerical work modelling the vertical distribution
76 of wave erosion as a direct function of tidal and therefore wave inundation frequency (Sunamura,
77 1975; 1977; Trenhaile and Layzell, 1981; Carr and Graff, 1982; Walkden and Hall, 2005; Walkden
78 and Dickson, 2008). At sites of harder rock cliffs where notches commonly do not develop, the
79 relationships between the vertical distribution of erosion, water level inundation frequency and
80 wave attack remain poorly constrained.

81 The challenges of obtaining relevant monitoring of coastal conditions has led to the use of
82 monitored cliff-top microseismic ground motions as a proxy for environmental forcing, based
83 upon the assumption that ground motion in part reflects the timing, magnitude and efficacy of
84 forcing (Adams et al., 2002; 2005; Young et al., 2011b; 2012; 2013; Dickson and Pentney, 2012;
85 Norman et al., 2013). Distinct microseismic frequencies describe particular types of conditions,
86 although frequency band widths vary by location dependent on local marine and
87 geomorphological characteristics. Wave impacts (e.g. Adams et al., 2002) and wind buffeting
88 (Norman et al., 2013) at the cliff generate high frequency shaking; local waves in shallow
89 nearshore waters generate ground motions of the same periods termed single frequency (SF)
90 microseisms; and double frequency (DF) microseisms are generated in open sea as a function of

91 wave superimposition and produce increased amplitudes (Adams et al., 2005; Young et al., 2011b;
92 2012; 2013; Norman et al., 2013). Energetic wave conditions during storms must be a key driver
93 of rock cliff erosion (e.g. Trenhaile, 1987; Bray and Hooke, 1997; Anderson et al., 1999; Walkden
94 and Hall, 2005), yet measuring their interaction with the cliff is problematic. Microseismics have
95 been shown able to act as a relative measure of marine and storm energy transfer to a cliff,
96 whereby ground motions can be used to examine relationships between storm characteristics,
97 energy and erosion.

98 Lim et al. (2011) explored the rate of seismic events recorded by a cliff-top geophone
99 above a ground acceleration trigger threshold in relation to rockfall activity monitored at monthly
100 intervals. No significant correlation was found between the number of seismic events and
101 resultant aggregate rockfall volume. However, a positive correlation between the monthly number
102 of seismic impacts and rockfalls occurring in the following month was observed, suggesting a
103 lagged effect, which the authors suggested may be an artefact of the monitoring interval used.
104 Using broadband seismometers over a 2-year period, Norman et al. (2013) derived the rate (μJ
105 hour^{-1}) of microseismic marine energy transfer, modulated by water level and wave climate, and
106 identified the vertical distribution of energy to the coast during the tidal cycle under various
107 conditions. This approach identified a notable difference in the timing of energy delivery as
108 compared to monitored or modelled tide-only inundation durations (Carr and Graff, 1982;
109 Trenhaile, 2000). The greatest rate of energy transfer, perhaps unsurprisingly, occurred during
110 the highest storm waters - periods that combined high tides, storm surge and large waves with
111 set-up. By implication, if the transfer of microseismic energy is suitable as a proxy for erosion,
112 then peak energy transfer during storms will be dominant in defining when and where erosion
113 occurs. The direct response of erosion to microseismic energy transfer and water level has
114 however not been examined until now.

115 The aim of this paper is to explore how best to represent conditions at the coast,
116 comparing microseismic motions, monitored far-field and modelled at-cliff conditions, and to use
117 these datasets to examine controls on the occurrence of erosion via rockfalls. Using a 2-year
118 monitoring dataset that includes 21 individual survey epochs of erosion data, relationships with
119 rockfalls from both the inundated cliff toe ('wet'), and the face above ('dry') are examined, to
120 consider the mechanisms driving erosion.

122 2. Study site

123 We focus here upon a section of 55 m high near-vertical Lower Jurassic mudstone, shale,
124 siltstone and sandstone cliff with an open northerly aspect on the east coast of N Yorkshire, UK
125 (Fig. 1a, b). The study builds upon previous monitoring of rockfalls and erosion at this site (Rosser
126 et al., 2007; 2013; Lim et al., 2010), which has a coast-parallel planar geometry *c.* 500 m from the
127 nearest bay or headland. The wide (*c.* 250 m during mean low spring tide), low-gradient ($< 1^\circ$)
128 rock foreshore and macrotidal conditions (*c.* 6 m range during spring tides) (Fig. 1c) generate
129 highly variable conditions at and near to the cliff, both through a single semi-diurnal tidal cycle,
130 and between seasons when conditions are greatly exacerbated by storms in the North Sea.

132 3 Methods

133 3.1. Field data

134 The following data were collected over *c.* 2-years (25 July 2008 – 28 June 2010); a period of
135 sufficient length to capture a range of coincident tidal / weather conditions at this site:

- 136 - Cliff microseismic motion in 3-axes, using a single 100 Hz Guralp 6-TD broadband seismometer,
137 installed within the cliff-top glacial till deposits (Fig. 1c);

138 - Data from the nearest available tide gauge combining water level and residuals from modelled
139 predictions (UK National Tide Gauge Network, Whitby [25 km south]). Hourly significant wave
140 heights and onshore and offshore wind speeds were obtained from an offshore buoy and
141 onshore weather station (CEFAS Wave Net, Teesside [20 km northwest from site]; UK Met
142 Office, Loftus [3 km west from site]) were collated. We refer to these data as 'distal' in the
143 following analysis.

144 - 3D scans were captured during low tides at 4 – 8 week intervals using a Trimble GS200
145 terrestrial laser scanner (TLS). The scanner ranging accuracy is 0.0015 m at 50 m. Data had a
146 minimum point spacing of 0.125 m across the monitored cliff.

148 **3.2 Wave modelling**

149 To approximate conditions local to the cliff, monitored distal waves and tide data were
150 modelled using a transformation based on Battjes and Stive (1985). This relatively simple
151 approach was used because detailed bathymetry data was not freely available for the area
152 between the buoy and the coast. The 30-minute data interval and single location of the offshore
153 wave buoy data meant that the resolution of input data was not sufficient for more complex wave
154 refraction models. Full details of the model are provided in Norman et al. (2013). The modelled
155 locations of breaking and surf zones match field observations. In the absence of monitoring data of
156 actual conditions the model output accuracy cannot be tested for this site. However, Battjes and
157 Stive (1985) compared outputs from this model for a similar site on the eastern coast of the North
158 Sea that experiences an analogous wave climate. They obtained a correlation coefficient of 0.98
159 between modelled and measured RMS wave heights, with an RMS normalised error of 6%.

161 **3.3 Data processing and analysis methods**

162 3.3.1 Rockfall and erosion data

163 TLS data was processed to derive rockfall volumes from sequential scans, which included
164 registering successive surveys, generating cliff-parallel surface elevation models and extracting
165 change. An object-oriented classification of individual rockfalls was used to extract rockfall
166 volumes (see: Lim et al. 2005; Rosser et al., 2005). Scans were sequentially registered with a root
167 mean square error of ± 0.1 m which, combined with the point spacing, meant that the minimum
168 volume of rockfalls detectable was *c.* 0.00156 m^3 . Rockfall data was aggregated by survey epoch to
169 describe rockfall location and failure geometry. For rockfalls in each epoch we calculate: total
170 volume, mean volume, standard deviation (σ) of the volume and maximum volume, plus the total
171 volumes within five rockfall size classes: class 1 $< 0.01 \text{ m}^3$; class 2 $0.01 \geq < 0.1 \text{ m}^3$; class 3 $0.1 \geq < 1$
172 m^3 ; class 4 $1 \geq < 10 \text{ m}^3$; and, 5 $\geq 10 \text{ m}^3$. In the analysis we hypothesize that the variability in
173 environmental drivers and resulting erosion response will be manifest between these survey
174 epochs.

175 The elevation of the boundary between the wet and dry sections of the cliff was estimated
176 by 'stacking' the maximum water heights over the 2-year monitoring period from modelled tides
177 and waves, including set-up. In the absence of a reasonable approximation for wave run-up and
178 splash on these cliffs, the maximum wave height was doubled. Whilst the distinction between
179 these two zones at fine-scale is arbitrary, here we seek only to derive a broad distinction between
180 the cliff face exposed to direct wave action (the bottom *c.* 5 m), and that above (the upper *c.* 50 m).

182 3.3.2 Seismic data

183 Seismic data was processed to derive signal power and energy in three frequency bands
184 that span the range of cliff top ground motions observed (50 – 0.1 Hz). These include: WI (12.5 –
185 50 Hz), representative of wind acting at the cliff face; HT (1.1 – 50 Hz), used as a proxy for wave
186 impacts on the cliff face during high spring tides or storm surges; and MS (1 – 0.1 Hz), which

187 describes microseisms generated both in the nearshore and at more distal locations within the
188 North Sea. We subsampled these bands to five discrete frequencies: 0.022 s (WI), selected because
189 WI and HT overlap and the HT signal is weakest at this frequency; 0.104 s (HT) selected because
190 this frequency experiences the highest powers without overlapping with WI; and three
191 frequencies for MS: 1 s (MS1) believed to represent a number of nearshore processes; 3 s (MS3)
192 the most frequently occurring wave period monitored at the wave buoy; and 5 s (MS5) the mean
193 wave period recorded at the wave buoy and also commonly is attributed to the peak amplitude in
194 the double frequency microseism range (e.g. McNamara and Buland, 2004). To demonstrate which
195 conditions dominate each of these frequencies, the signal power was regressed against the
196 monitored and modelled marine and wind datasets. Signal power was used because the rate of
197 energy transfer, rather than the total energy transferred, was found to provide greater detail and
198 differentiation as to when, and therefore how, energy is transferred to the cliff. This helps to
199 identify the processes generating the ground motions.

200 To undertake analysis of the microseismic motion with the erosion data the mean,
201 maximum and total (non-normalised for time) seismic energy of each survey epoch was
202 calculated, for each frequency, as a proxy for the energy available to drive erosion. A degree of
203 background noise in each of these frequencies may be included within these values (notably HT,
204 discussed below). However, examination of spectrograms demonstrates that signal amplitude is
205 generally dominated by fluctuations coincident with changes in environmental conditions (see
206 Norman et al., 2013).

207

208 **3.3.3 Environmental data**

209 The monitored and modelled environmental data were re-sampled to the means, totals and
210 extremes for each survey epoch where appropriate. The following variables were used in the
211 analysis: tide height and residuals at the Whitby tide gauge; wave height at the offshore wave

212 buoy; modelled water surface elevation and inundation duration above the cliff toe combining
213 tide, surge, wave and set-up heights; and wind velocity. Regression analysis to derive the
214 coefficient of determination (r^2 for simple regression models (one independent variable) and R^2
215 for the multiple regression models) was used to test for and describe the relationships between
216 the concurrent environmental and microseismic conditions and erosion. Only the statistically
217 significant relationships ($p < 0.001$) are presented.

219 **4. Results**

220 **4.1 Marine and weather conditions**

221 **4.1.1 Monitored and modelled environmental conditions**

222 The coast is storm-dominated during the winter months, with stronger winds, larger waves
223 and larger tide residuals (Fig. 2a-c). The relatively limited fetch of the North Sea restricts wave
224 height and period, although waves that have travelled over greater distances can enter the North
225 Sea from the North Atlantic. More than 80% of significant wave heights monitored at the buoy are
226 ≤ 2 m, and maximum recorded wave height at the buoy was 6.45 m (Fig. 2c). The mean recorded
227 wave period at the buoy is 5 s and maximum was 20 s. Longer wave periods occur in winter
228 months (Fig. 2d).

229 The intertidal zone extends across the 250 m wide foreshore (Fig. 1c). As the mean high
230 neap water level is just below the cliff toe, only during high spring tides is any of the cliff face
231 inundated during still water conditions (Fig. 1c). Modelled tide, surge, wave and set-up heights at
232 the cliff have been combined to estimate total water level above the cliff toe (Fig. 2e). Maximum
233 modelled water level reaches 2.9 m above the cliff toe, 1.4 m higher than tidal inundation alone.
234 The resulting change in inundation is important in terms of not only the amount of time wave
235 energy is transferred directly to the cliff, but also where on the cliff face this occurs. The modelled

236 combined water elevations (Fig. 2e) differ significantly to distal wave heights at the buoy (Fig. 2c)
237 due to the transformation of waves through the shallow waters of the nearshore and foreshore. In
238 the absence of monitored foreshore waves the modelled marine heights provide a useful estimate
239 of the temporal variability of conditions at the cliff.

240

241 **4.1.2 Microseismic cliff ground motions**

242 The mean hourly signal power (spectrograms) (Fig. 3ai, bi) and energy observed within the
243 WI and MS ground motion frequencies (Fig. 3aii, bii) reflect the variability of the monitored
244 marine and wind conditions (Fig. 2a-c). More energetic wind (WI) (Fig. 3b) and wave (MS1, 3 & 5)
245 conditions (Fig. 3a) occurred during autumn and winter months (October – March). HT
246 frequencies are strongly modulated by tide height, and so vary ostensibly independently of season
247 (Fig. 3b). Within the MS spectrogram the maximum wave period during the summer is 8 s and
248 increases during winter (Fig. 3ai), indicating the occurrence of longer period swell waves
249 generated by more stormy winter winds and waves (Fig. 2a-d). Highest powers in the microseism
250 band also occur in winter, in the period range 3 – 8 s (Fig. 3ai). These are the most frequently
251 occurring wave periods recorded at the buoy (Fig. 2d); however, this is also the period range of DF
252 microseisms which have larger amplitudes, so the higher powers in this range likely reflects both
253 sources. Of the 3 MS frequencies examined, the 5 s signal mean hourly power shows the most
254 pronounced seasonal variation, as this period captures swell waves generated by distal storms
255 (Fig. 3aii).

256

257 **4.1.3 Microseismic cliff motions as proxies for environmental conditions**

258 Regression analysis between the monitored and modelled environmental conditions and
259 the ground motion frequencies was undertaken. Linear regression between wave characteristics

260 at the buoy, winds and modelled waves at the cliff toe were undertaken to determine whether the
261 signals were related to winds or wave processes at the cliff, or more distally. The highest r^2 values
262 for the WI frequency are generated by onshore winds ($r^2 = 0.6$) (Fig. 4). In contrast the HT and MS
263 frequencies have higher r^2 values with waves rather than winds (Fig. 4). The highest r^2 value
264 (0.21) for HT demonstrates that cliff toe waves are the most important (Fig. 4); however, the low
265 r^2 value indicates other factors are likely to contribute significantly to this signal. In the
266 spectrogram for this frequency band (Fig. 3bi) there is a constant noise source that overlaps with
267 this frequency, believed to be generated by an industrial pump 150 m from the seismometer. The
268 r^2 values for the three MS frequencies indicate that the MS signals relate best to waves at the buoy
269 (Fig. 4); however, the r^2 values decrease with increasing period (MS1 $r^2 = 0.67$; MS3 $r^2 = 0.44$; and
270 MS5 $r^2 = 0.21$). This indicates that as wave period increases, waves at the buoy contribute less to
271 the microseismic signal at the cliff. As the 3 and 5 s MS periods sit within the DF microseism range,
272 this may indicate that these signals are partially generated by DF mechanisms further offshore.

273 To better constrain the nature of wind or wave conditions that generate each of the five
274 frequency bands, multiple regression analysis considering monitored wind velocity (from all
275 directions and onshore winds only), tide, waves at the buoy and modelled wave and set-up heights
276 at the cliff, was undertaken. The combinations of variables that produced the highest statistically
277 significant R^2 values are presented (Tab. 1). Each of these produces a higher R^2 value than the
278 simple pair-wise regression models (Fig. 4). The WI model ($R^2 = 0.72$) (Tab. 1) comprises onshore
279 wind velocity, which the associated beta coefficients demonstrate make the greatest contribution
280 in the model, and wave and set-up heights at the cliff, representing the overlap with the HT band.
281 For the HT frequency adding set-up heights to the wave heights at the cliff increases the R^2 value
282 (0.53) (Tab. 1) from the model of wave heights alone (0.21) (Fig. 4). Wave set-up heights make the
283 greatest contribution to HT (Tab. 1), indicating the importance of wave breaking at the cliff in
284 generating this signal. Norman et al. (2013) observed that the HT signal was generated only

285 during high spring tides or surges that enabled large waves to impact directly against the cliff face.
286 The significant variables and high R^2 values of both the pair-wise (0.67) (Fig. 4) and multiple
287 linear regression (0.80) models (Tab. 1) for the MS1 signal indicate that both marine conditions at
288 the cliff and those more widely contribute to this signal. The significance of set-up at the cliff
289 indicates 1 s signals are partially generated by processes associated with wave breaking, also
290 observed by McCreery et al. (1993). As the minimum wave period recorded at the buoy was 2 s,
291 the 1 s signal may therefore represent the superposition of 2 s waves or the local generation of 1 s
292 wind waves landward of the buoy, supported by the increased significance of onshore winds in
293 the MS1 model (Tab. 1). The significance of the addition of onshore winds to the MS3 model ($R^2 =$
294 0.58) (Tab. 1) and winds from all directions to the MS5 model ($R^2 = 0.27$) (Tab. 1) may be used to
295 infer the location of waves generating these microseisms as proximal to the coast, with the 3 s
296 signal generated in the nearshore and the 5 s signal further afield.

297

298 **4.2 Rockfall characteristics**

299 Rockfalls occurred across the cliff face, with small failures occurring the most frequently in
300 both wet and dry sections of the cliff (Fig. 5a). 31,987 rockfalls were observed during the
301 monitoring period, ranging in volume from 0.00156 to 12.73 m³. Mean erosion rate across the
302 whole cliff over the monitoring period, estimated by averaging total rockfall volume over the
303 monitored area, is 0.024 m yr⁻¹ (Tab. 2). The total volume of rockfalls, normalised by time (days),
304 was typically greater in the dry zone, reflecting the larger surface area (Tab. 2, Fig. 6c), yet higher
305 rates of erosion occurred in the wet zone (Tab. 2, Fig. 6b). Mean individual rockfall volume and
306 standard deviation in volume were greater in the wet zone, with the exception of June – July 2009
307 when the largest single failure observed occurred in the dry zone above (Tab. 2; Fig. 5a; Fig. 6a).

308 There is a strong geological control on the character of individual rockfalls. Small rockfalls
309 were released along bedding planes in the sandstone and siltstone (Fig. 5a). The greatest sum of

310 rockfall volumes was observed in the mudstone in the lower 20 m of the cliff face (Fig. 5a), the
311 lowest 5 m of which is directly inundated by the sea. The wider joint spacing in the mudstone
312 releases larger rockfalls. Above the mudstone, the exposed shale is friable, producing small rock
313 fragments. There is apparently a clustering of rockfalls over successive months (see example in
314 Fig. 5a and b). Subsequent rockfalls occur around the edges of scars of earlier failures, most
315 evident in the shale and mudstones.

316 The largest total volume of rockfalls per epoch, normalised by the number of days, occurs
317 in winter months (October – February) (Fig. 6c), yet erosion rates (Fig. 6b) and individual rockfall
318 characteristics (Fig. 6a) vary between survey epochs. This may in part be explained by the
319 combination of factors necessary to prepare and then trigger rockfalls, defining their
320 characteristics and timing. In addition, the monthly resolution of our data may mean that
321 individual rockfalls may reflect multiple superimposed events.

322

323 **4.3 Observed environmental controls on rockfalls**

324 **4.3.1 Monitored and transformed marine and weather variables**

325 The modelled water heights above the cliff toe demonstrate stronger significant
326 relationships (r^2) with rockfalls across the whole cliff face, and with more rockfall characteristics,
327 than the distally monitored tide, wave and wind variables (Fig. 7). The modelled water heights
328 allow the more energetic, stormy seas, and the resulting direct wave impacts upon the cliff, to be
329 distinguished from those less energetic periods. The highest r^2 values are for the mean water
330 heights with mean rockfall volume ($r^2 = 0.53$) and the total rockfall volume in size class 4 ($r^2 = 0.55$)
331 (Fig. 7). These results suggest that more energetic marine conditions at the cliff generate more
332 rockfalls of larger volume. Regression with the inundation duration produces fewer, weaker r^2
333 values (0.21 – 0.36) suggesting that water height (incorporating tides, surge, waves and set-up)
334 better represents the available marine energy at the cliff. Maximum tide height and residuals at

335 the tide gauge both relate to the mean rockfall volume ($r^2 = 0.27$ and 0.49 , respectively) and total
336 volume in class size 4 ($r^2 = 0.23$ and 0.35 , respectively) (Fig. 7). Wind velocity and wave heights
337 monitored at the buoy also have significant relationships with a range of rockfall measures ($r^2 =$
338 $0.22 - 0.45$), the highest r^2 value occurring between total wave heights and total rockfall volume
339 ($r^2 = 0.45$). Whilst these relationships indicate the influence of these conditions on rockfall
340 volumes, geological strength and structure are also key in determining failure volume (e.g. Lim et
341 al., 2010).

342 In the wet zone of the cliff, the distally-monitored mean tide height and maximum wind
343 velocity also produce significant, albeit low, r^2 values with rockfall variables (0.22 and 0.27
344 respectively) (Fig. 7). Modelled mean water height above the cliff toe again produces significant r^2
345 values with total volume (0.30), maximum volume (0.26) and the total volume of rockfalls in size
346 class 4 (0.27). The tide residuals at the gauge and wave heights at the buoy demonstrate an
347 influence on a range of rockfall characteristics with the highest r^2 values of 0.54 between
348 maximum tidal residual and mean rockfall volume, and 0.38 between total wave buoy height and
349 maximum rockfall volume. Interestingly, both the distal tide residuals and wave buoy heights are
350 found to relate to the highest number of rockfall descriptors (Fig. 7). These results imply that tide
351 residuals and wave heights monitored away from the cliff generate more energetic and hence
352 erosive conditions at the coast more widely, and these are replicated at the cliff during high tides
353 and surges.

354 In the dry zone, the distal maximum and total wave heights at the buoy relate with total
355 and mean rockfall volumes and with total rockfall volumes in class size 3, although significant r^2
356 values are low ($r^2 < 0.26$) (Fig. 7). Total wind velocity also influences total rockfall volume ($r^2 =$
357 0.30) and mean rockfall volume ($r^2 = 0.37$). The modelled combined water height above the cliff
358 toe and inundation duration relate to more of the rockfall characteristics from across the dry zone
359 and with the highest r^2 values ($r^2 = 0.22 - 0.61$). The total water height produces the highest r^2 of

360 0.61 with mean rockfall volume, and along with the mean water height has relationships with the
361 highest number of rockfall variables (Fig. 7). The water heights above the cliff toe describe high
362 tide conditions with energetic waves where both set-up and storm surge may increase the at-cliff
363 water level, facilitating increased wave energy transfer to the cliff face and coast (Norman et al.,
364 2013). These relationships indicate an indirect influence of marine conditions on rockfalls higher
365 up the cliff face. Possible indirect marine influences are cliff shaking of the cliff rock mass (e.g.
366 Adams et al., 2005), winds or spray that influence the exposed cliff face above more widely and act
367 in tandem with energetic marine conditions, or potentially that marine erosion rapidly propagates
368 up-cliff (e.g. Rosser et al., 2013).

369

370 **4.3.2 Microseismic variables**

371 Each of the microseismic frequency bands derive statistically significant relationships with
372 rockfall characteristics from across the whole cliff ($r^2 = 0.20 - 0.53$) (Fig. 8). Similar to the
373 environmental variables, microseismic data produce significant r^2 values with total, mean and
374 standard deviation of rockfall volume, and notably with the total volume of rockfalls in class size
375 4. HT, which has been shown to be a proxy for high-tide wave impacts at the cliff, produces the
376 highest coefficient of determination of the microseismic variables (0.56) and relates to the most
377 rockfall characteristics (Fig. 8), reflecting both rockfall size and yield.

378 In the wet zone, HT produces significant, yet relatively low, r^2 values with the maximum
379 and total observed rockfall volume and the total volume of rockfalls in classes 2 and 4 (0.20 –
380 0.29) (Fig. 8). WI and MS5 both relate to mean rockfall volume producing the highest r^2 values
381 (0.38 and 0.36, respectively), and with other measures of rockfall volume ($r^2 = 0.19 - 0.31$).
382 Relationships between HT and rockfalls within the wet zone indicate a direct influence of cliff face
383 wave conditions on erosion. The significance of WI and MS5 suggests that, as measures of regional

384 storm conditions, these frequencies also relate to conditions at the cliff that bear some control on
385 erosion.

386 Rockfalls from the dry zone relate to microseismic variables known previously to
387 represent marine conditions at or near to the cliff: HT and MS1 (Fig. 8), matching the results of the
388 environmental variables regressions. Both HT and MS1 demonstrate an influence on a number of
389 measures of rockfall volume, with both producing the highest r^2 value with the total volume of
390 rockfalls in class 4 (0.52 and 0.37, respectively). In addition, the maximum energy values observed
391 in MS3 and MS5 relate to total volume in class 1 ($r^2 = 0.24$ and 0.35 , respectively). These results
392 support those derived for the dry zone rockfalls and monitored and modelled environmental
393 variables, suggesting that the whole cliff face, and not just the wet zone, responds over the time-
394 scale investigated here (months) to concurrent marine conditions.

395

396 **4.4 Water level, energy transfer and erosion**

397 Given the dependence of rockfalls and erosion upon marine conditions demonstrated, we
398 explore the vertical distribution of material loss as a function of inundation duration and marine
399 energy transfer (Fig. 9). This is achieved by integrating the monitored time-series data by water
400 elevation. The relationships above indicate that water level above the cliff toe provides a better
401 measure of the erosive marine energy than inundation duration (Fig. 7). Comparing inundation
402 duration with the mean microseismic energy transfer across the frequency band 0.14 – 50 Hz
403 (0.02 – 7s), which incorporates the frequencies of interest to this study, it is evident that whilst
404 energy transfer increases, the duration of inundation decreases with increasing water level (Fig.
405 9). Increased energy transfer occurs during large storms with peak water levels as a combined
406 function of tides, surges, waves and set-up, but such peak water levels remain infrequent. During
407 more frequently observed water levels, energy flux is reduced, whereby conditions include tide-
408 only water heights during calm seas, and more shallow water depths limit wave propagation to

409 the cliff toe. From our monitoring data, the greatest erosion depths occur within the wet zone,
410 with up to 20% of the monitored width of cliff eroding to depths over 1 m, compared to 0.5 m in
411 the dry zone (Fig. 9 and 10). Mean and max erosion depths in the wet zone are ~0.4 m and 2.7 m
412 respectively, compared to ~0.2 m and 1.3 m in the dry zone (Fig. 9 and 10). The foci in erosion
413 depth appears to correspond with the elevations of the most regularly observed inundation level
414 during low energy conditions, and at the less frequent but increased water levels achieved during
415 high energy conditions (Fig. 9). However, these depths occur across only 1% of the monitored cliff
416 width and are not representative of depths across the whole site (Fig. 9). The cliff profiles from the
417 start and end of the monitoring period demonstrate an absence of notching associated with either
418 inundation duration or the most energetic water levels and the vertical distribution of erosion
419 throughout the wet zone varies across the cliff width (Fig. 11).

421 **5 Discussion**

422 **5.1 Environmental conditions at the cliff**

423 Microseismic cliff motions and modelled cliff face water heights incorporating tides, surges,
424 waves and set-up, have been found to be useful measures of the marine conditions that interact
425 directly with a cliff and result in erosion. Examination of these variables provides insight into the
426 relative transfer of marine energy to the cliff, and how this varies through time. As the datasets
427 considered here reflect the combined effects of tides, winds and waves and the transformation
428 through shallow nearshore waters, they provide an improved measurement of conditions at the
429 cliff as compared to distally monitored data.

430 Using a relatively simple analysis to test a similarly logical and simple set of relationships,
431 the strongest links have been observed between transformed marine variables and microseismic
432 cliff motions and cliff rockfalls, rather than those using distally measured marine and weather
433 data. The difficulty in relating environmental conditions to erosion may therefore be in part a

434 function of how and where such monitoring data is collected and analysed. Whilst we have been
435 unable to test the accuracy of the modelled wave heights at the monitored cliff, the regressions
436 with the microseismic ground motions and rockfalls indicate that the wave model estimates are
437 reliable as relative measures of conditions at the cliff. The relationships between modelled marine
438 conditions and rockfalls reflect observations elsewhere, where distally measured marine
439 conditions that have been transformed to estimate conditions at the cliff have been found to relate
440 to observed erosion (Ruggiero et al., 2001; Sallenger et al., 2002; Collins and Sitar, 2008). The
441 modelled water levels at the cliff toe produce slightly higher r^2 values when regressed against
442 rockfall volumes than the microseismic variables, which may suggest these variables can more
443 clearly represent marine conditions that erode the cliff material.

444 Young et al. (2013) questioned whether cliff microseismic motions can be used as proxies
445 for marine energy transfer by, due to the potential overlap with signals generated by other
446 seismic sources at the coast. Whilst there is evidence of signal overlap, both between
447 characterised frequency bands and with local and distal noise sources, the regression analysis
448 demonstrates a significant proportion of cliff top ground motion frequencies to be generated by
449 local wind (WI), marine conditions (HT, MS1, MS3), and distal waves (MS5). These relationships
450 have not previously been quantified, rather the generating processes have been identified using
451 visual comparisons of time-series of ground motion and concurrent marine conditions (e.g. Adams
452 et al., 2005; Young et al., 2011b; 2012; Norman et al., 2013). This approach is also important for
453 determining signal source, particularly for those signals which are highly variable, such as tides.
454 All five microseismic frequencies show statistically significant relationships with rockfall
455 occurrence and characteristics. The marine microseismic frequencies HT and MS1, observed to be
456 generated by waves breaking at the cliff have the strongest relationships with a greater number of
457 rockfall characteristics. Comparing these relationships with those of Lim et al. (2011), it is evident

458 that the detail provided by analysis of specific frequencies holds benefits over and above velocity
459 or acceleration trigger or threshold-based analysis across a wider bandwidth.

460 Measuring a range of marine and wind processes operating over different spatial scales
461 using one instrument at a cliff-top, rather than from the cliff face, foreshore or offshore is
462 advantageous. Young et al. (2013) demonstrated that nearshore wave processes generate coastal
463 microseismic motions on sandy shores, indicating that such approaches can be applied across a
464 range of coastal settings. There are, however, limitations to this approach. First, microseismic
465 monitoring requires minimal local background noise to guarantee a sufficient signal-to-noise ratio
466 (McNamara and Buland, 2004). This study demonstrates that using individual frequencies that are
467 less influenced by such noise can help address this problem. The variable attenuation of different
468 ground motion frequencies (Lowrie, 1997) and the complex travel paths and seismic velocities
469 renders such data as a relative rather than an absolute measure. In examining the signal sources
470 and relationships with observed erosion, and whilst accepting microseismic data as a relative
471 measurement, this has not been found to be problematic. Young et al. (2013) also observed that
472 signal characteristics generated by the same processes at different coastlines can vary, making
473 comparisons between multiple sites challenging. Wave energy, which acts as a catalyst to many
474 coastal processes, is manifest in our monitoring data, so again is considered as a suitable proxy for
475 these processes.

477 **5.2 Environmental controls on hard rock cliff failure**

478 The data show that as well as erosion of the toe, marine and atmospheric forcing at the
479 coast have some influence on failures from the face. Importantly, even over the relatively short
480 monitoring period considered here (2 years), the driver-erosion link is apparent, and may indicate
481 the conditions that are significant as drivers of cliff erosion over the longer-term.

482 In the inundated zone, rockfall volumes relate to both environmental and microseismic
483 conditions, reflecting the action of waves and storm surges at the cliff, but also more general
484 widespread conditions. The absence of a notch at water levels associated with either inundation
485 duration or peak microseismic energy transfer, and the variable distribution of erosion both up
486 the cliff profile and along the monitored width, reflects the complex spatial distribution of
487 rockfalls observed here, and other rock coasts (e.g. Teixeira, 2006; Rosser et al., 2007; 2013;
488 Young et al., 2009a; Lim et al., 2010). The distribution of erosion within the wet zone likely
489 reflects spatial and temporal variations in both wave energy focussing and cliff rock strength. The
490 wave energy focus on the cliff depends on the effects of nearshore and foreshore bathymetry
491 (Komar, 1998; Trenhaile, 2000; Trenhaile and Kanyaya, 2007; Ogawa et al., 2011). More locally to
492 the cliff, foreshore roughness and cliff toe morphology determine where waves, surf, run-up and
493 splash are concentrated. Variations in erosive effectiveness are also determined by local rock
494 strength, and with an homogeneous cliff toe geology, such as at the study site, rock structure that
495 can be exploited by hydraulic action during wave impact and removal of the fractured rock is key
496 (Trenhaile 1987; Sunamura, 1992), and will also influence rockfall geometry and volume (e.g.
497 Rosser et al., 2007). An increased inundation frequency is assumed to equate to increased erosion
498 over time (e.g. Trenhaile, 2000; Walkden and Hall, 2005; Trenhaile, 2009; 2011; Ashton et al.,
499 2011), which may be applicable to cliffs in softer materials and less energetic environments;
500 however, our data suggest that for hard rock cliffs it is the available energy that is important in
501 defining the rate and net volume of erosion, which is not determined by inundation duration
502 alone.

503 The observed relationships indicate that these cliffs will respond to environmental
504 changes. In demonstrating the erosive effectiveness of different marine energy scenarios, these
505 results are useful for considering how hard rock cliffs may respond to future changes in sea level
506 and wave climate. The results suggest that for hard rock coastal cliffs, models of inundation

507 duration may not adequately define the erosion response to increasing sea level and thus wave
508 energy transfer.

509 For both the marine and the microseismic variables considered, both the largest number
510 and strongest relationships were obtained for rockfalls from the whole cliff face, combining both
511 wet and dry zones. Erosion of the dry cliff face is typically attributed to: a) subaerial processes,
512 unique to this relatively dry, essentially non-saline environment (Emery and Kuhn, 1982;
513 Sallenger et al., 2002); b) time-dependent deformation and failure of the rockmass (Rosser et al,
514 2007; Styles et al., 2011; Stock et al., 2012); or c) a combination of the two (Rosser et al., 2013). As
515 wave-cut notches do not form at this site, we speculate that marine triggering of failures from the
516 upper cliff face may also result from either microseismic cliff motion generated by waves,
517 particularly during energetic storm conditions, or by rapid (i.e. over timescales shorter than the c.
518 monthly monitoring period used here) up-cliff propagation of marine triggered rockfalls (e.g.
519 Rosser et al., 2013). The latter process falls beneath the temporal resolution of our survey, yet the
520 former is supported by the relationships between distal environmental variables and cliff ground
521 motions with various measures of rockfall occurrence shown.

522 Adams et al. (2005) proposed that the repeated flexure by marine-generated microseismic
523 motions generate stresses sufficient to develop micro-fractures, decreasing the bulk rock mass
524 strength. In a study of the effectiveness of this process on the cliffs studied here, Brain et al.
525 (2014) suggested that the amplitudes of ground motion are insufficient to cause ongoing
526 microcracking (i.e. 'damage'). In the absence of this process, the correlations between the
527 microseismic frequency bands and the rockfall characteristics across the whole cliff face shown
528 here may imply that rather than causing damage, ground motions generated by marine and wind
529 processes may play a role in the final release of rockfalls in previously-damaged sections of the
530 cliff. This mechanism may help to explain the triggering of rockfalls from the upper parts of the

531 cliff, which may previously have been considered to be disconnected from marine processes at the
532 cliff toe (e.g. Rosser et al., 2005).

533 Whilst the r^2 values generated in this study are statistically significant, they remain
534 moderate (<0.6), which may partially be explained by the strong geological controls on rockfalls
535 and erosion. The analysis of the data over the monitoring epochs (4 – 8 weeks) implies that
536 observed failures may occur as a near-immediate response to forcing or as a lagged response
537 within the time-scale of the sampling period. The temporal resolution of the rockfall dataset
538 however does not enable us to distinguish the exact timing of rockfalls and the instantaneous
539 conditions; at present we are only able to obtain a first-order assessment of the relative
540 importance of the direct and indirect triggering of rockfalls and erosion.

541

542 **6 Conclusions**

543 Cliff-top microseismic motions and modelled cliff toe marine conditions have been found to
544 provide a useful measure of conditions and processes at the cliff toe and a relative measure of
545 energy transfer to the coast. In the absence of monitored foreshore wave data, the microseismic
546 and modelled marine datasets have enabled examination of relationships between conditions at
547 the cliff and erosion. Statistically significant relationships were obtained between marine and
548 microseismic variables and rockfalls, indicating a complex control of marine and wind processes
549 on hard rock coastal cliff erosion. Relationships between distally-monitored marine conditions
550 and rockfalls demonstrate that more widespread stormy marine conditions are replicated at the
551 coast when tides and surges enable the sea to reach the cliff. The strongest relationships were
552 found with rockfalls from across the whole cliff face, rather than solely within the inundated wet
553 zone. The marine influence on erosion therefore extends indirectly above the inundated zone. We
554 hypothesise that in addition to acting as proxies for forcing, the microseismic cliff motions

555 themselves potentially hold some influence on the timing and nature of erosion in those cliff
556 rockfalls otherwise preconditioned for release.

557 Our results demonstrate, not surprisingly, a marine control on cliff toe erosion. Perhaps
558 more surprisingly, the impact of conditions that vary over 2 years when aggregated over periods
559 of one to two months can explain, to a certain degree, the variations in erosion via rockfalls. Whilst
560 cliff toe marine conditions are found to relate to rockfalls from across the whole cliff face, within
561 the wet zone the distribution of erosion is not determined by inundation duration or heights
562 associated with maximum energy transfer. Instead, erosion of the hard rock cliff toe varies up-cliff
563 and alongshore, which we attribute to variations in the local bathymetry and therefore waves, and
564 the cliff rock mass strength. These results suggest that for hard rock cliffs the relationship
565 between inundation duration, energy transfer and erosion of hard rock cliffs is more complex than
566 indicated by tidal inundation models alone.

567

568 **Acknowledgements**

569 The authors gratefully acknowledge the continued support for this research from
570 Cleveland Potash Ltd. The seismic network was provided by NERC's SEIS-UK (loan no. 879), and
571 the guidance of Alex Brisbane, David Hawthorn and Victoria Lane. We also acknowledge the
572 support of Michael Lim, Sam Waugh, and John Barlow in the collection of the field data. Many
573 thanks also to two anonymous reviewers for their constructive feedback.

574

575 **References**

- 576 Adams, P.N., Anderson, R.S., Revenaugh, J., 2002. Microseismic measurement of wave-energy
577 delivery to a rocky coast. *Geology* 30, 895-898.
- 578 Adams, P.N., Storlazzi, C.D., Anderson, R.S., 2005. Nearshore wave-induced cyclical flexing of sea
579 cliffs. *Journal of Geophysical Research-Earth Surface* 110.
- 580 Anderson, R.S., Densmore, A.L., Ellis, M.A., 1999. The generation and degradation of marine
581 terraces. *Basin Research* 11, 7-19.
- 582 Ashton, A.D., Walkden, M.J.A., Dickson, M.E., 2011. Equilibrium responses of cliffed coasts to
583 changes in the rate of sea level rise. *Marine Geology* 284, 217-229.
- 584 Battjes, J.A., Stive, M.J.F., 1985. Calibration and verification of a dissipation model for random
585 breaking waves. *Journal of Geophysical Research-Oceans* 90, 9159-9167.
- 586 Brain, M.J., Rosser, N.J., Norman, E.C., Petley, D.N., 2014. Are microseismic ground displacements a
587 significant geomorphic agent? *Geomorphology* 207, 161-173.
- 588 Bray, M.J., Hooke, J.M., 1997. Prediction of soft-cliff retreat with accelerating sea-level rise. *Journal*
589 *of Coastal Research* 13, 453-467.
- 590 Brooks, S. M., Spencer, T., Boreham, S., 2012. Deriving mechanisms and thresholds for cliff retreat
591 in soft-rock cliffs under changing climates: Rapidly retreating cliffs of the Suffolk coast, UK.
592 *Geomorphology* 153-4, 48-60.
- 593 Carr, A.P., Graff, J., 1982. The tidal immersion factor and short platform development - discussion.
594 *Transactions of the Institute of British Geographers* 7, 240-245.
- 595 Collins, B.D., Sitar, N., 2008. Processes of coastal bluff erosion in weakly lithified sands, Pacifica,
596 California, USA. *Geomorphology* 97, 483-501.
- 597 Dickson, M.E., Pentney, R., 2012. Micro-seismic measurements of cliff motion under wave impact
598 and implications for the development of near-horizontal shore platforms. *Geomorphology* 151,
599 27-38.

600 Duperret, A., Genter, A., Mortimore, R.N., Delacourt, B., De Pomerai, M.R., 2002. Coastal rock cliff
601 erosion by collapse at Puys, France: The role of impervious marl seams within chalk of NW
602 Europe. *Journal of Coastal Research* 18, 52-61.

603 Emery, K.O., Kuhn, G.G., 1982. Sea cliffs - their processes, profiles, and classification. *Geological*
604 *Society of America Bulletin* 93, 644-654.

605 Kogure, T., Matsukura, Y., 2010. Critical notch depths for failure of coastal limestone cliffs: case
606 study at Kuro-shima Island, Okinawa, Japan. *Earth Surface Processes and Landforms* 35, 1044-
607 1056.

608 Komar, P.D., 1998. *Beach processes and sedimentation*, 2nd ed. Prentice Hall, Upper Saddle River,
609 N.J.

610 Lim, M., Petley, D.N., Rosser, N.J., Allison, R.J., Long, A.J., Pybus, D., 2005. Combined digital
611 photogrammetry and time-of-flight laser scanning for monitoring cliff evolution. *Photogrammetric*
612 *Record* 20, 109-+.

613 Lim, M., Rosser, N.J., Allison, R.J., Petley, D.N., 2010. Erosional processes in the hard rock coastal
614 cliffs at Staithes, North Yorkshire. *Geomorphology* 114, 12-21.

615 Lim, M., Rosser, N.J., Petley, D.N., Keen, M., 2011. Quantifying the Controls and Influence of Tide
616 and Wave Impacts on Coastal Rock Cliff Erosion. *Journal of Coastal Research* 27, 46-56.

617 Lowrie, W., 1997. *Fundamentals of geophysics*. Cambridge University Press, Cambridge ; New
618 York, NY, USA.

619 McNamara, D.E., Buland, R.P., 2004. Ambient noise levels in the continental United States. *Bulletin*
620 *of the Seismological Society of America* 94, 1517-1527.

621 Norman, E.C., Rosser, N.J., Brain, M.J., Petley, D.N., Lim, M., 2013. Coastal cliff-top ground motions
622 as proxies for environmental processes. *Journal of Geophysical Research-Oceans* 118, 6807-6823.

623 Ogawa, H., Dickson, M.E., Kench, P.S., 2011. Wave transformation on a sub-horizontal shore
624 platform, Tatapouri, North Island, New Zealand. *Continental Shelf Research* 31, 1409-1419.

625 Pierre, G., Lahousse, P., 2006. The role of groundwater in cliff instability: an example at Cape
626 Blanc-Nez (Pas-de-Calais, France). *Earth Surface Processes and Landforms* 31, 31-45.

627 Rosser, N., Lim, M., Petley, D., Dunning, S., Allison, R., 2007. Patterns of precursory rockfall prior to
628 slope failure. *Journal of Geophysical Research-Earth Surface* 112.

629 Rosser, N.J., Brain, M.J., Petley, D.N., Lim, M., Norman, E.C., 2013. Coastline retreat via progressive
630 failure of rocky coastal cliffs. *Geology* 41, 939-942.

631 Rosser, N.J., Petley, D.N., Lim, M., Dunning, S.A., Allison, R.J., 2005. Terrestrial laser scanning for
632 monitoring the process of hard rock coastal cliff erosion. *Quarterly Journal of Engineering Geology*
633 *and Hydrogeology* 38, 363-375.

634 Ruggiero, P., Komar, P.D., McDougal, W.G., Marra, J.J., Beach, R.A., 2001. Wave runup, extreme
635 water levels and the erosion of properties backing beaches. *Journal of Coastal Research* 17, 407-
636 419.

637 Sallenger, A.H., Krabill, W., Brock, J., Swift, R., Manizade, S., Stockdon, H., 2002. Sea-cliff erosion as a
638 function of beach changes and extreme wave runup during the 1997-1998 El Nino. *Marine*
639 *Geology* 187, 279-297.

640 Stephenson, W.J., Kirk, R.M., 2000. Development of shore platforms on Kaikoura Peninsula, South
641 Island, New Zealand - Part one: The role of waves. *Geomorphology* 32, 21-41.

642 Stock, G., Martel, S., Collins, B., Harp, E., 2012. Progressive failure of sheeted rock slopes: The 2009
643 - 2010 Rhombus Wall rock falls in Yosemite Valley, California, USA. *Earth Surface Processes and*
644 *Landforms* 37, 546 - 561.

645 Styles, T.D., Coggan, J.S., Pine, R.J., 2011. Back analysis of the Joss Bay Chalk Cliff Failure using
646 numerical modelling. *Engineering Geology* 120, 81-90.

647 Sunamura, T., 1975. Laboratory study of wave-cut platform formation. *Journal of Geology* 83, 389-
648 397.

649 Sunamura, T., 1977. Relationship between wave-induced cliff erosion and erosive force of waves.
650 *Journal of Geology* 85, 613-618.

651 Sunamura, T., 1992. *Geomorphology of rocky coasts*. J. Wiley, Chichester; New York.

652 Teixeira, S.B., 2006. Slope mass movements on rocky sea-cliffs: A power-law distributed natural
653 hazard on the Barlavento Coast, Algarve, Portugal. *Continental Shelf Research* 26, 1077-1091.

654 Trenhaile, A.S., 1987. *The geomorphology of rock coasts*. Clarendon Press, Oxford.

655 Trenhaile, A.S., 2000. Modeling the development of wave-cut shore platforms. *Marine Geology*
656 166, 163-178.

657 Trenhaile, A.S., 2009. Modeling the erosion of cohesive clay coasts. *Coastal Engineering* 56, 59-72.

658 Trenhaile, A.S., 2011. Predicting the response of hard and soft rock coasts to changes in sea level
659 and wave height. *Climatic Change* 109, 599-615.

660 Trenhaile, A.S., Kanyaya, J.I., 2007. The role of wave erosion on sloping and horizontal shore
661 platforms in macro- and mesotidal environments. *Journal of Coastal Research* 23, 298-309.

662 Trenhaile, A.S., Layzell, M.G.J., 1981. Shore platform morphology and the tidal duration factor.
663 *Transactions of the Institute of British Geographers* 6, 82-102.

664 Walkden, M., Dickson, M., 2008. Equilibrium erosion of soft rock shores with a shallow or absent
665 beach under increased sea level rise. *Marine Geology* 251, 75-84.

666 Walkden, M.J.A., Hall, J.W., 2005. A predictive Mesoscale model of the erosion and profile
667 development of soft rock shores. *Coastal Engineering* 52, 535-563.

668 Young, A.P., Adams, P.N., O'Reilly, W.C., Flick, R.E., Guza, R.T., 2011b. Coastal cliff ground motions
669 from local ocean swell and infragravity waves in southern California. *Journal of Geophysical*
670 *Research-Oceans* 116.

671 Young, A.P., Flick, R.E., Gutierrez, R., Guza, R.T., 2009a. Comparison of short-term seacliff retreat
672 measurement methods in Del Mar, California. *Geomorphology* 112, 318-323.

673 Young, A.P., Guza, R.T., Adams, P.N., O'Reilly, W.C., Flick, R.E., 2012. Cross-shore decay of cliff top
674 ground motions driven by local ocean swell and infragravity waves. *Journal of Geophysical*
675 *Research-Oceans* 117.

676 Young, A.P., Guza, R.T., Dickson, M.E., O'Reilly, W.C., Flick, R.E., 2013. Ground motions on rocky,
677 cliffed, and sandy shorelines generated by ocean waves. *Journal of Geophysical Research-Oceans*
678 118, 6590-6602.

679 Young, A.P., Guza, R.T., Flick, R.E., O'Reilly, W.C., Gutierrez, R., 2009b. Rain, waves, and short-term
680 evolution of composite seacliffs in southern California. *Marine Geology* 267, 1-7.

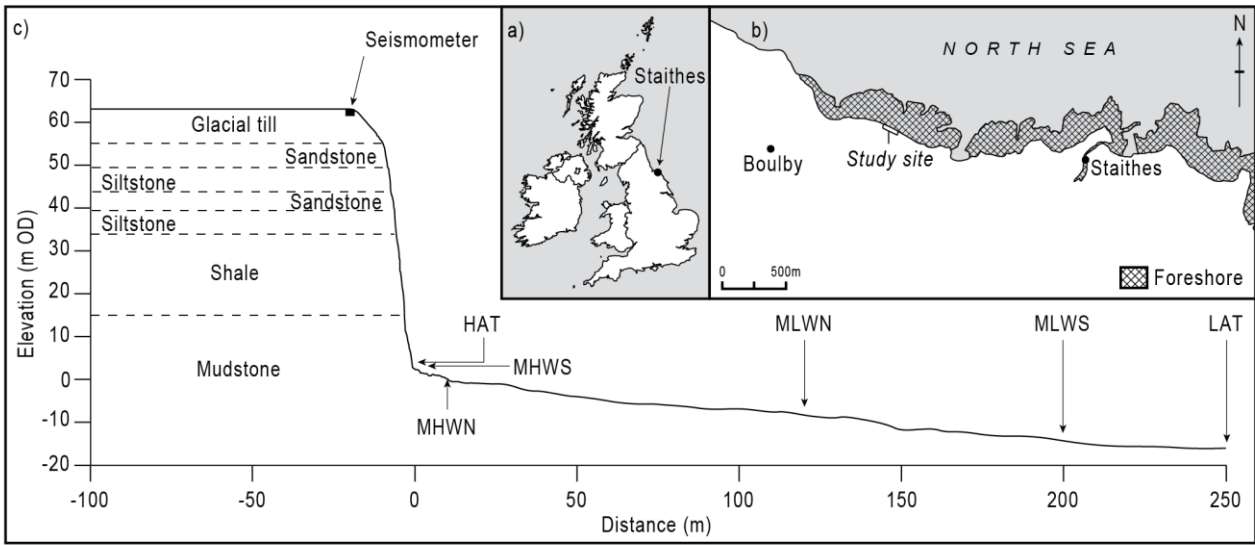
681 Young, A.P., Guza, R.T., O'Reilly, W.C., Flick, R.E., Gutierrez, R., 2011a. Short-term retreat statistics
682 of a slowly eroding coastal cliff. *Natural Hazards and Earth System Sciences* 11, 205-217.

683

684

685

686



688

689 **Figure 1: a & b)** Study site 1.5 km west of the village of Staithes, on the North Yorkshire coast, UK.

690 The foreshore platform extent at low spring tide is shown by the hatched area; **c)** Cliff and

691 intertidal foreshore cross-profile, showing the seismometer position 20 m back from the vertical

692 cliff face. The x-axis is defined from the cliff toe, which is at an elevation of 1.6 m OD. Tidal mean

693 and extreme elevations are labelled as: HAT = highest astronomical tide; MHWS = mean high

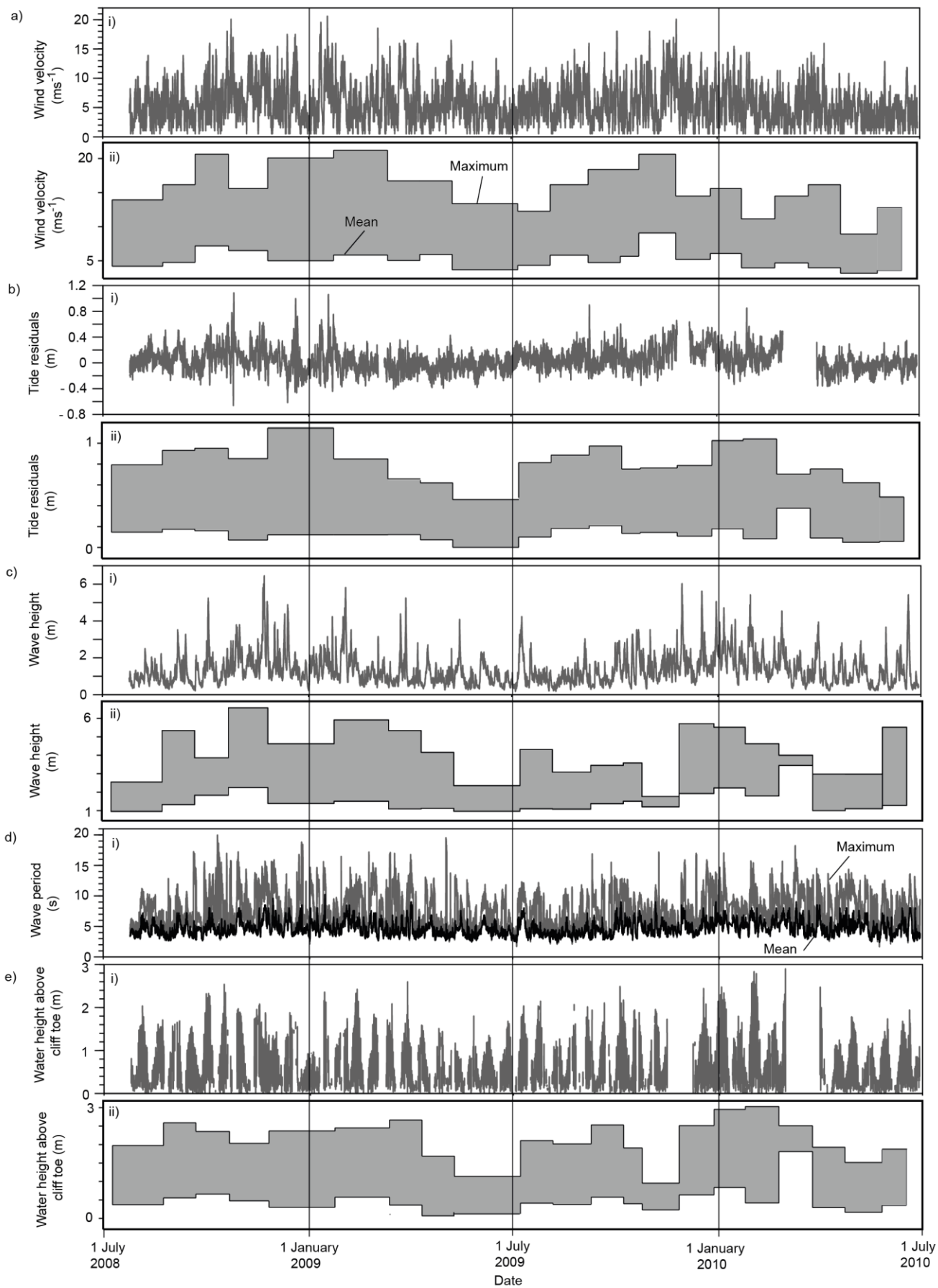
694 water spring; MHWN = mean high water neap; MLWN = mean low water neap; MLWS = mean low

695 water spring; LAT = lowest astronomical tide. A simplified geological description illustrates the

696 near-horizontally bedded structure of the cliff.

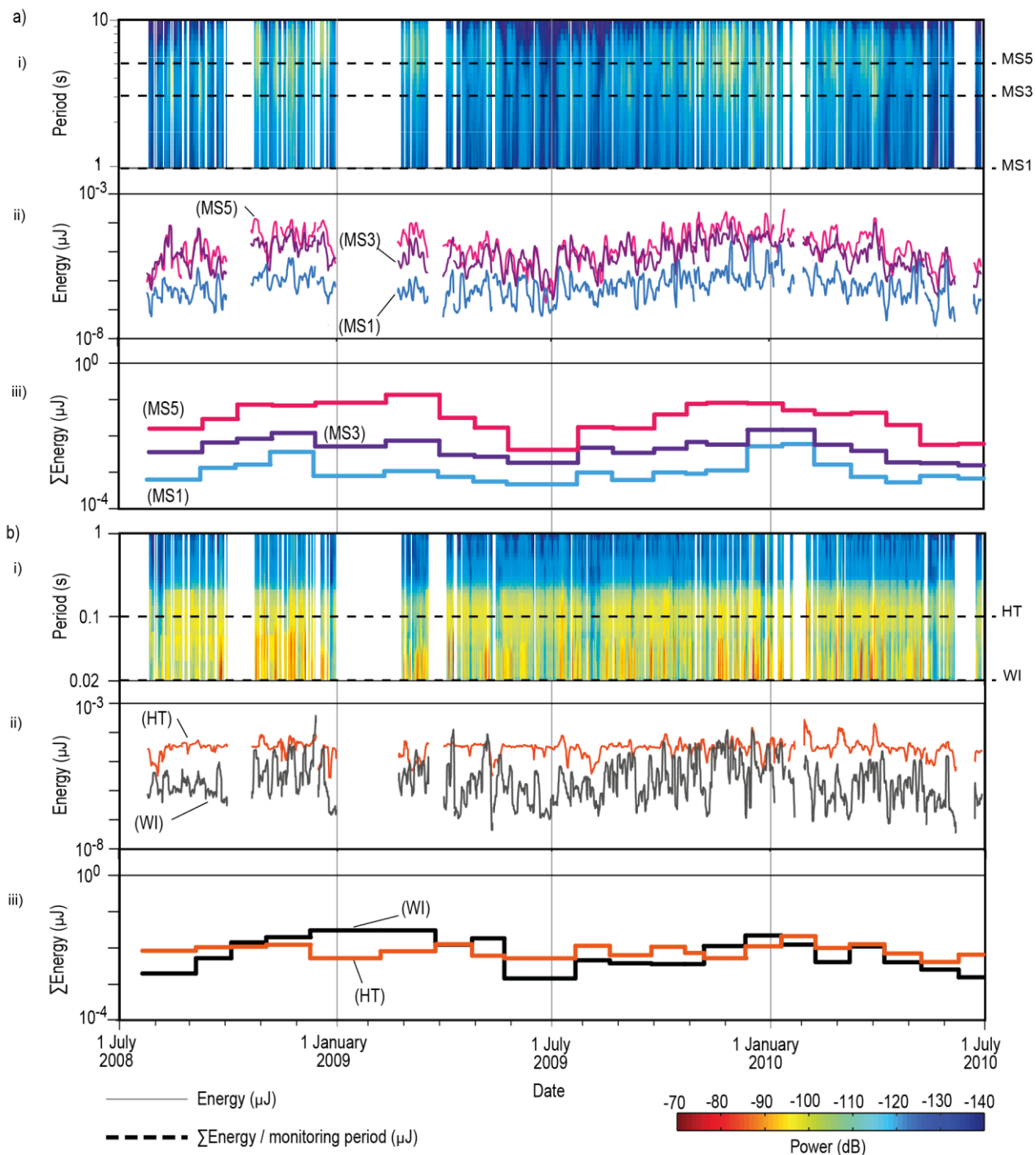
697

698



700 **Figure 2: i)** Monitored/modelled environmental variables over the 2-year monitoring period, and
701 **ii)** maximum (shaded area top edge) and mean (shaded area lower edge) values per survey epoch.
702 Note that the width of each epoch is bound by the TLS monitoring survey dates. **a)** Monitored
703 wind velocity; **b)** Monitored tide residuals at the tide gauge; **c)** Monitored significant wave heights
704 at the wave buoy; **d)** Monitored wave periods at the buoy; and **e)** Modelled water heights above
705 the cliff toe incorporating tides, surges, waves and set-up. Gaps in the data are due to equipment
706 failure.

707



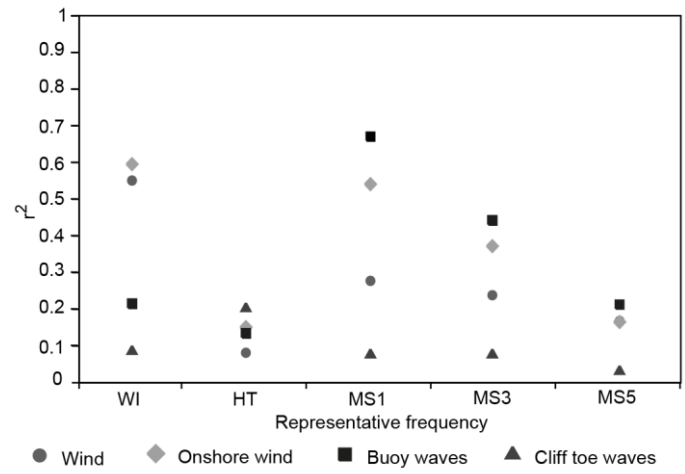
708

709

710 **Figure 3: a) i)** Spectrogram of microseismic signal power, showing data captured between
 711 periods 10 s & 1 s. Horizontal dashed lines show the subsampled frequency bands MS1, MS3 and
 712 MS5. White areas show times where the instrument failed to record data. **ii)** Hourly mean signal
 713 energy in the MS1, MS3 and MS5 frequency bands. **iii)** Sum of the energy recorded in MS1, MS3
 714 and MS5 band within each survey epoch. **b) i)** Spectrogram of microseismic signal power, showing

715 data captured between periods 1 s & 0.02 s. Horizontal dashed lines show the subsampled
716 frequency bands WI and HT. **ii)** Hourly mean signal energy in the WI and HT frequency bands. **iii)**
717 Sum of the energy recorded in WI and HT, band within each survey epoch. Gaps in the data are
718 due to equipment failure.

719

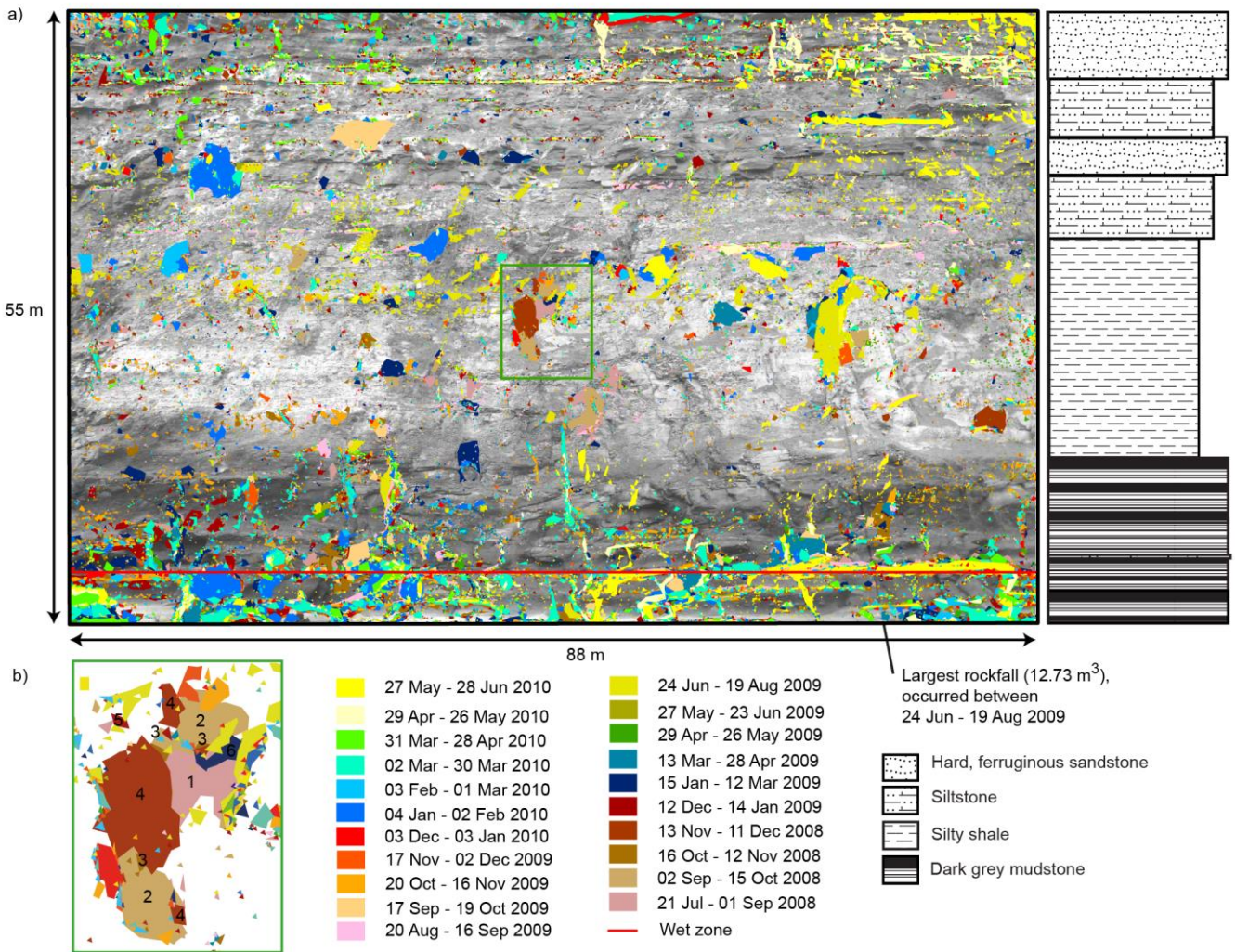


720

721

722 **Figure 4:** r^2 values from simple linear regression models between the representative frequencies
 723 of each frequency band (WI = 0.022 s; HT = 0.104 s; MS1= 1 s, MS3 = 3 s and MS5 = 5 s) and wind
 724 velocity from all directions, onshore wind velocity, wave height at the buoy and wave height at the
 725 cliff.

726

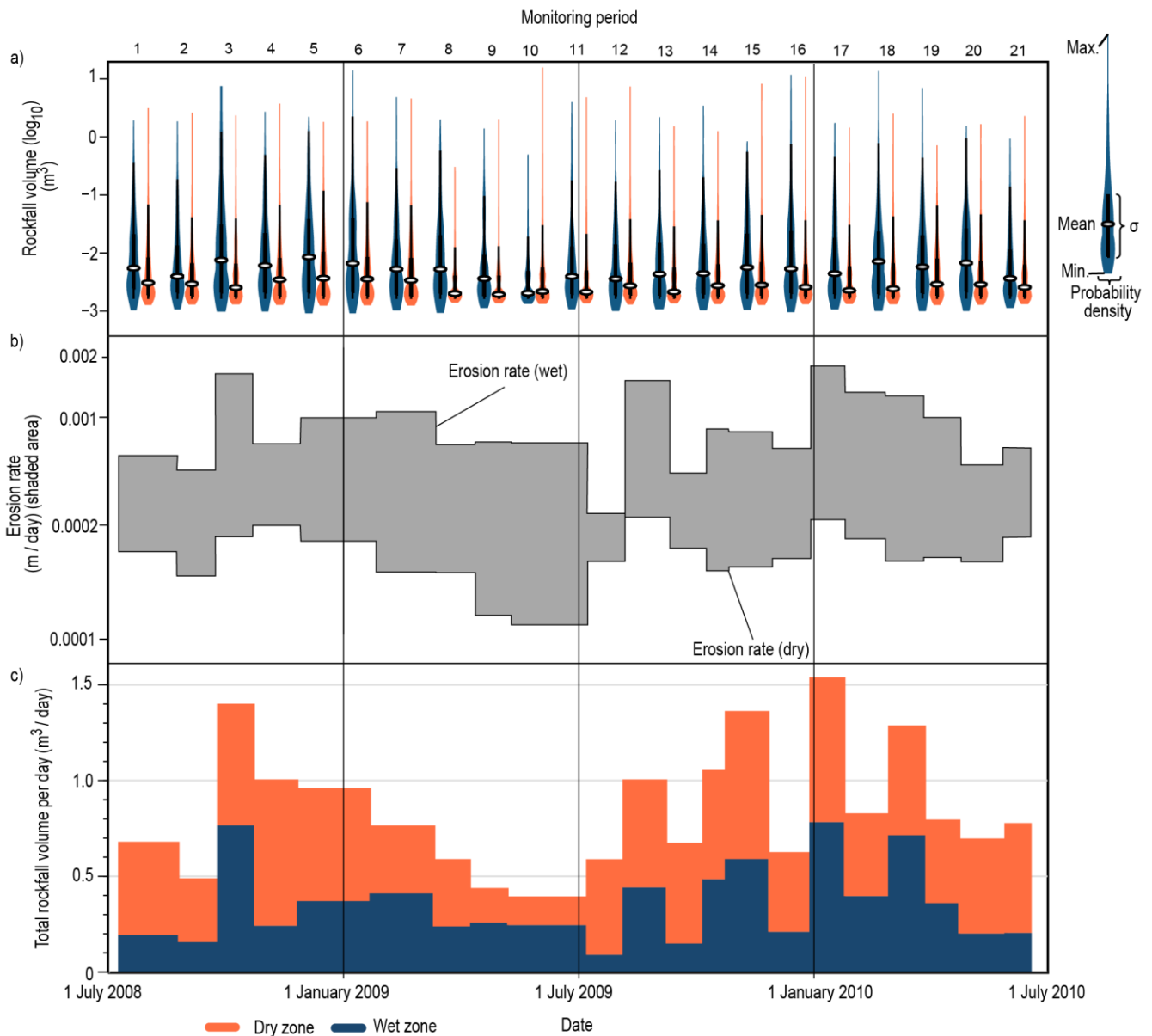


727

728

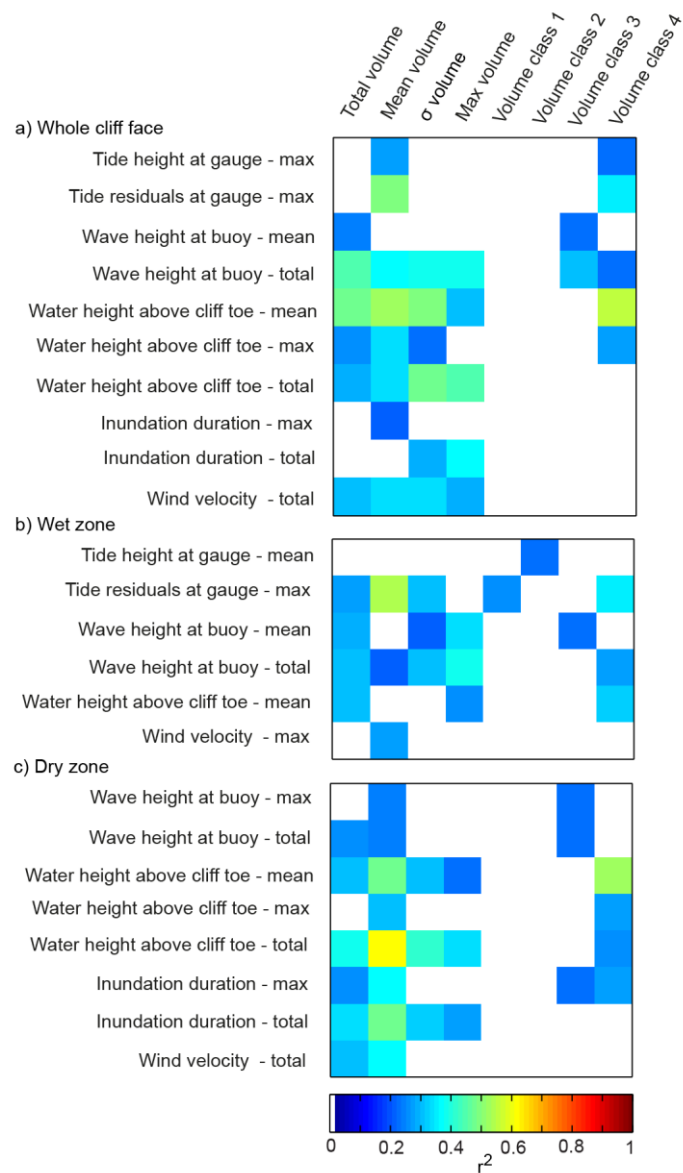
729 **Figure 5: a)** Monitored rockfalls captured across the cliff face between 25 July 2008 to 28 June
 730 2010. Each rockfall scar is color-coded by survey period, overlaid upon a monochrome
 731 orthoimage of the cliff for context. The red line delimits the wet from the dry sections of the cliff
 732 face. A close-up of the green box from the centre of the cliff is presented in **b)** showing clustering
 733 of larger rockfalls that occurred in the first six epochs (numbered) of the monitoring period.

734



735

736 **Figure 6: a)** ‘Violin plot’ showing the range, probability density, mean, standard deviation and
 737 maximum of rockfall volumes per survey epoch from the wet (blue) and dry (orange) sections of
 738 the monitored cliff face. Note that the width of each subplot is delimited by survey epoch, not date.
 739 **b)** Erosion rate for each survey epoch (shaded area). The top edge of the shaded area is the
 740 erosion rate in the wet zone, and the lower edge the erosion rate in the dry zone. **c)** The top of the
 741 orange and blue colored bars show the total volume of rockfalls, standardised by day, during each
 742 survey epoch across the whole cliff face. The orange bars are the total volume standardised by day
 743 for the dry zone only, and the blue the wet zone only. Note that the width of each period (b and c)
 744 is bound by the monitoring survey dates (x-axis).

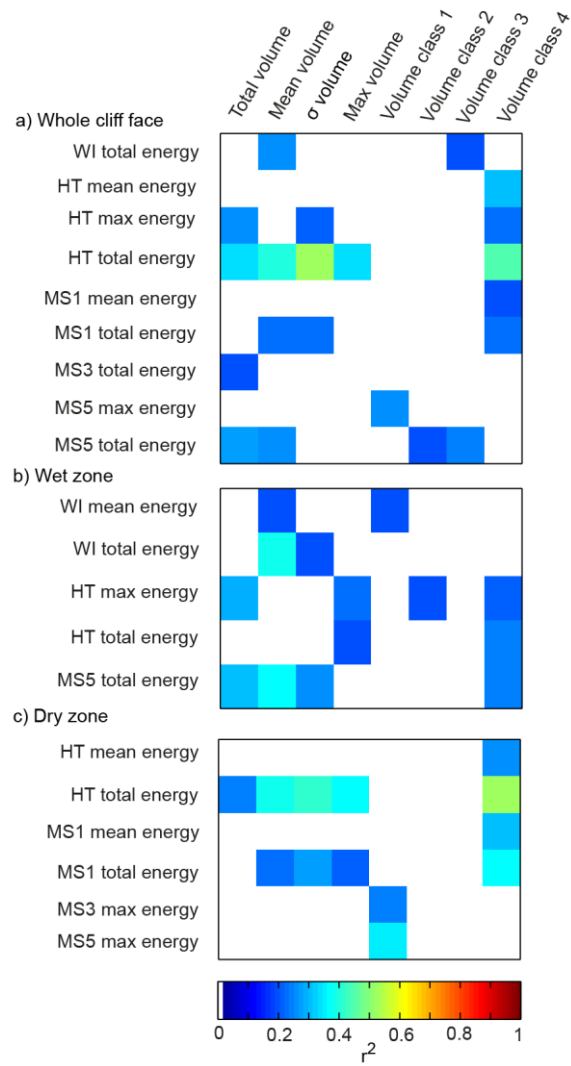


745

746

747 **Figure 7:** Statistically significant r^2 values from regression analyses between distally monitored
 748 and transformed environmental variables with rockfalls from across: **a)** the whole cliff face; **b)** the
 749 wet zone; and **c)** the dry zone. Only statistically significant relationships are presented in colour.

750

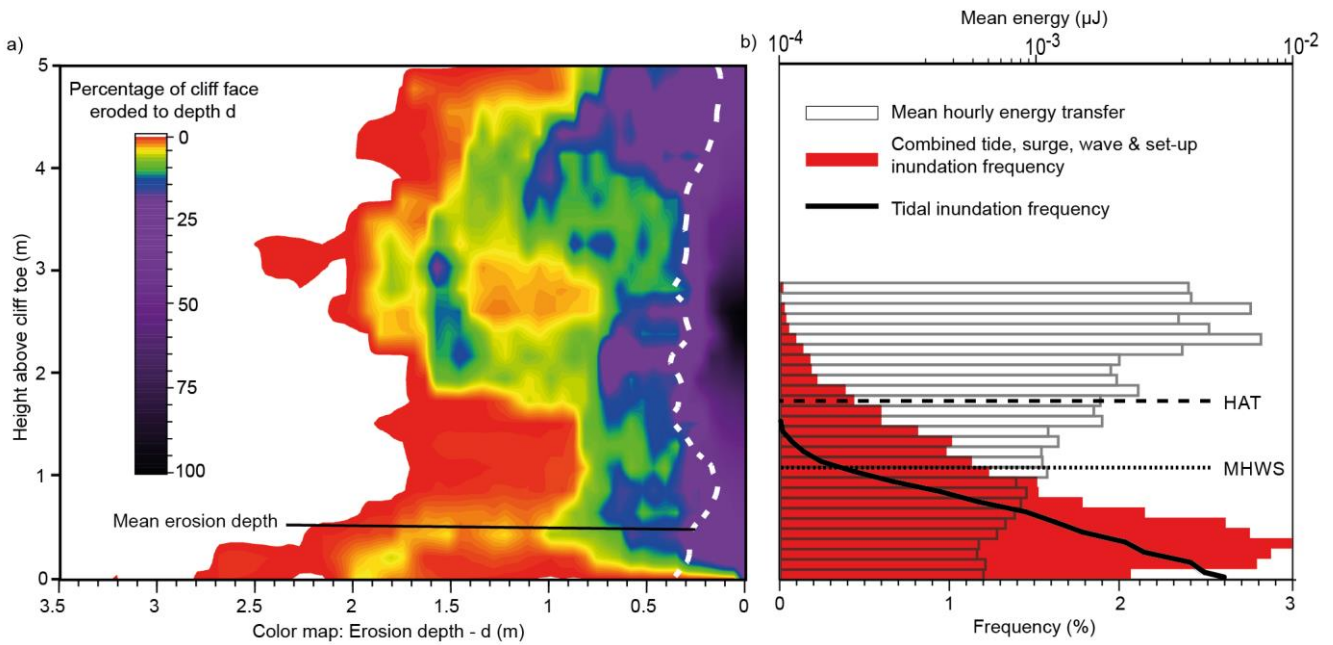


751

752

753 **Figure 8:** Statistically significant r^2 values from regression analyses between cliff-top
 754 microseismic variables with rockfalls from across: **a)** whole cliff face; **b)** the wet zone; and **c)** the
 755 dry zone. Only statistically significant relationships are presented in colour.

756

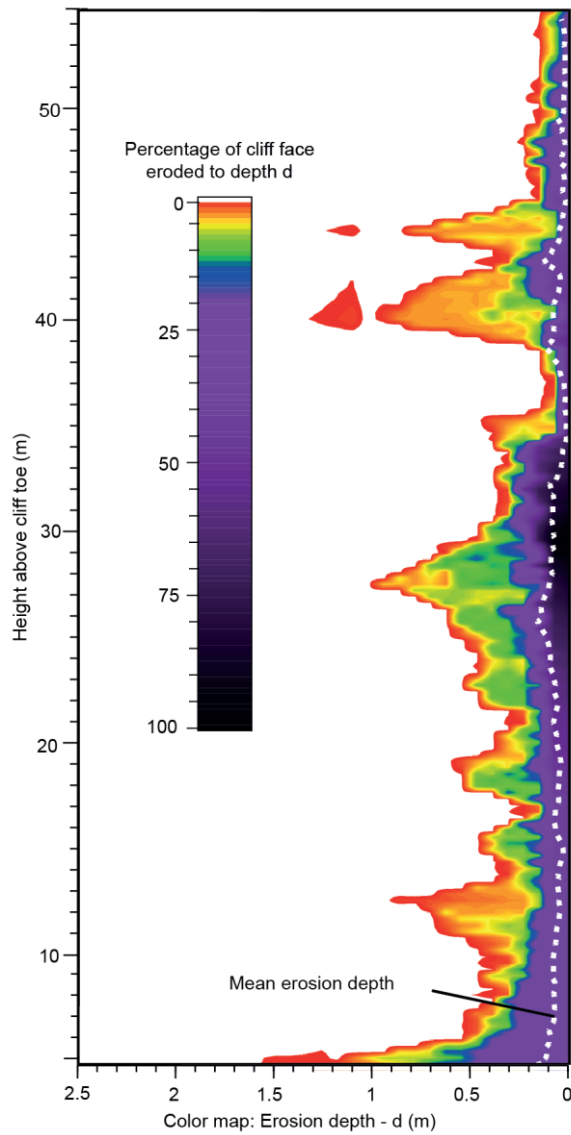


757

758

759 **Figure 9: a)** Colored profile shows the distribution of erosion depths with height up the cliff from
 760 0 to 5 m above the cliff toe, the 'wet' zone. Data is binned into 0.1 m vertical bins, colored
 761 according to the percentage of the monitored width of the cliff-face eroding to depth d (x-axis).
 762 The white dashed line shows the mean erosion depth. The left edge of the colored area denotes
 763 the maximum erosion depth. **b)** The mean hourly energy transfer across the frequency band 0.14
 764 – 50 Hz (0.02 – 7 s), modulated by still water level in 0.1 m vertical increments (hollow horizontal
 765 bars). Red horizontal bars (0.1 m vertical increments) show the relative frequency of inundation
 766 by combined tide, surge, wave and set-up. The solid black line shows the tidal inundation
 767 frequency.

768

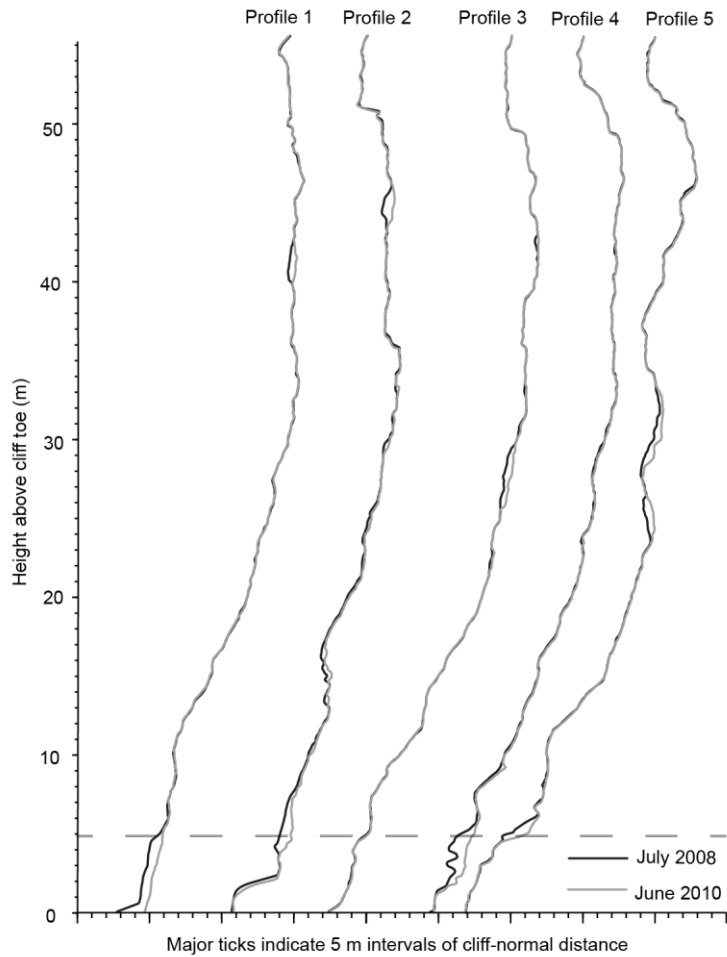


769

770

771 **Figure 10:** Colored profile shows the distribution of erosion depths with height up the cliff from 5
 772 to 55 m above the cliff toe, the 'dry' zone. Data is binned into 0.1 m vertical bins, colored according
 773 to the percentage of the monitored width of the cliff-face eroding to depth d (x-axis). The white
 774 dashed line shows the mean erosion depth. The left edge of the colored area denotes the
 775 maximum erosion depth.

776



777

778

779 **Figure 11:** Change in cliff profile morphology over the monitoring period. Five profiles have been
 780 selected at 15 m intervals moving from left to right across the monitored width of cliff. The initial
 781 profile in July 2008 is in black, and the final profile in June 2010 is in grey. The x-axis shows
 782 distance from the cliff top position of each profile, with the major ticks at 5 m intervals. The
 783 dashed line delimits the wet and dry zones.

784

785

786 **Table 1:** The R^2 values and regression beta coefficients from the multiple linear regression
 787 models that had the strongest (statistically significant) relationship with the representative
 788 frequencies of the three frequency bands (WI = 0.022 s; HT = 0.104 s; MS1= 1 s, MS3 = 3 s and MS5
 789 = 5 s). The beta coefficients are a standardised measure of the relative strength of each of the
 790 independent variables in the regression model in explaining the seismic signals' frequency power.
 791 They are measured in standard deviations of the seismic power.

792

Representative frequency	R²	Significant variables	Beta coefficients
WI	0.72	Onshore wind	0.45
		Cliff toe waves	0.25
		Cliff toe set-up	0.41
HT	0.53	Cliff toe waves	0.51
		Cliff toe set-up	0.58
MS1	0.80	Onshore wind	0.20
		Cliff toe waves	0.29
		Cliff toe set-up	0.68
MS3	0.58	Onshore wind	0.13
		Waves at buoy	0.67
MS5	0.27	Wind from all directions	0.26
		Waves at buoy	0.35

793

794

795 **Table 2:** Rockfall statistics for the whole cliff, plus the wet and dry sections, over the 2-year
796 monitoring period.

797

Section of cliff	Number of rockfalls	Total volume (m³)	Mean volume (m³)	Standard deviation (m³)	Maximum volume (m³)	Minimum volume (m³)	Annual retreat rate (m yr⁻¹)
Whole cliff	31,987	235.621	0.0180	0.163	12.732	0.00156	0.0243
Wet zone	5,736	79.535	0.0409	0.249	8.139	0.00156	0.1076
Dry zone	26,621	159.131	0.0128	0.130	12.732	0.00156	0.0178

798